Electronic states in heterostructures formed by ultranarrow layers

2012 J. Phys.: Condens. Matter 24 445010

(http://iopscience.iop.org/0953-8984/24/44/445010)

J. Phys.: Condens. Matter **24** (2012) 445010 (8pp) doi:10.1088/0953-8984/24/44/445010

Electronic states in heterostructures formed by ultranarrow layers

F T Vasko and V V Mitin

Department of Electrical Engineering, University at Buffalo, Buffalo, NY 14260-1920, USA

E-mail: fedirvas@buffalo.edu

Received 9 June 2012, in final form 20 September 2012
Published 9 October 2012
Online at stacks.iop.org/JPhysCM/24/445010

Abstract

Low-energy electronic states in heterostructures formed by ultranarrow layers (single or several monolayers in thickness) are studied theoretically. The host material is described within the effective mass approximation and the effect of ultranarrow layers is taken into account within the framework of the transfer matrix approach. Using the current conservation requirement and the inversion symmetry of an ultranarrow layer, the transfer matrix is evaluated through two phenomenological parameters. The binding energy of localized state, the reflection (transmission) coefficient for the single ultranarrow layer case, and the energy spectrum of the superlattice are determined by these parameters. The spectral dependency of absorption due to photoexcitation of electrons from localized states into minibands of the superlattice is determined by the ultranarrow layer characteristics. Such a dependency can be used for verification of the transfer matrix and should modify the characteristics of optoelectronic devices with ultranarrow layers. Comparison with experimental data shows that the effective mass approach is not valid for the description of ultranarrow layers.

(Some figures may appear in colour only in the online journal)

1. Introduction

Multi-layer heterostructures are widely used in different devices, such as bi- or monopolar heterostructure lasers, photodetectors and solar cells, see reviews [1] or [2, 3] and [4], respectively. Thicknesses of layers in such structures are vary widely, starting from an ultranarrow layer (UNL) of thickness a or Na for single or several monolayer structures, e.g. the case of the quantum dot sheets with ultranarrow wetting layers, see [5]. Here a is the monolayer thickness and $N = 1, 2, \ldots$ is the number of monolayers; for an InAs monolayer in a GaAs matrix $a \simeq 3.25$ Å. The case of $N \gg 1$ corresponds to a wide well or a barrier which is described in the framework of the effective mass approximation (EMA) or the **kp**-method supplied by appropriate boundary conditions at heterointerfaces [6]. Early in the eighties, similar approaches were used for the description of abrupt heterojunctions between different bulk semiconductors, see [7, 8] and references in [8]. The electronic properties of short-period superlattices (SL), i.e. heterostructures formed by periodic UNLs, were studied experimentally and numerically based on different approximations, see [9, 10], respectively. These approaches determine the energy spectra of SL only, but they are not suitable for consideration of transport and optical phenomena. To the best of our knowledge, the effect of UNLs on these phenomena was not considered in detail because the effective mass approximation is not valid over scales $\sim a$. If a heterostructure includes UNLs, one should consider it as a new object which is described by boundary conditions added to the EMA equations at UNL positions, $z = z_0$. Because heterostructures with UNLs are routinely used in different optoelectronic devices without an investigation of the peculiarities mentioned, it is important and timely to develop an adequate theory of electronic states at the UNL and to perform a verification of the UNL's parameters.

In this paper we consider an UNL placed at $\{z_0\}$, by applying the effective mass approximation (or the **kp**-method) for the host material, at $z \neq z_0$, and by using boundary conditions at $z \to z_0$ which describe modifications of envelope functions at UNL. In order to describe low-energy electron states, with energies in the vicinity of the conduction band extremum, in heterostructures formed by UNLs we employ the EMA approximation in the host material and the boundary conditions at UNLs written through the transfer matrix. The

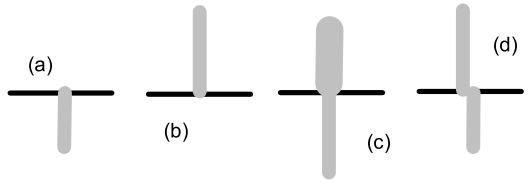

Figure 1. Band diagrams of UNLs enclosed by host semiconductor for: (a) well-like case with $|\tau| < 1$, (b) barrier-like case with $\tau > 1$, and (c) combined case with $\tau < -1$, and (d) non-symmetric case. Here gray regions correspond to microscopic potentials in different kinds of UNLs and τ is the diagonal element of the transfer matrix, see equation (5) .

parameters of such a matrix are restricted by the current conservation condition and the boundary conditions are written below for a symmetric UNL, see figures 1(a)–(c) (the case of non-symmetric UNL, shown in figure 1(d) should be considered elsewhere). Depending on the dimensionless diagonal element of the transfer matrix τ introduced in equations (5), one should separate UNLs into three categories: (i) a well-like UNL with $|\tau| < 1$, (ii) a barrier-like UNL with $\tau > 1$, and (iii) a non-conventional UNL with $\tau < -1$. These cases are sketched in figures 1(a)–(c), respectively, where thicknesses of layers (filled in by gray) are comparable to a. While the cases (i) or (ii) correspond to the EMA description of a narrow well or a barrier at $Na \to 0$ [11], a non-conventional UNL has no simple EMA analogy. In general, it is convenient to characterize the transfer matrix by a dimensionless phase, Θ, and a characteristic wavevector, K, see equations (5)–(7). The wavevector K (or the characteristic energy $E_K = (\hbar K)^2/2m$) describes the strength of the UNL potential while the factor Θ is connected with phase relations between the wavefunction and its derivative at the UNL. The phenomenological parameters K and Θ determine a character of low-energy states together with the effective mass (or parameters of the **kp**-method, if the energy is comparable to the gap of the host semiconductor) and they should be determined from experimental data.

Here we have evaluated the transfer matrix, which is written through the parameters Θ and K, and have considered electronic properties of different types of single UNLs as well as SL formed by UNLs. We calculated the binding energy of the localized state at a single UNL, which appears to be the allowed state for the cases (i) and (iii) and to be the forbidden state for the barrier-like case (ii). The energy-dependent reflection (transmission) coefficient is found when considering the scattering of electron on the UNL. For the SL formed by UNLs, we analyze the energy spectrum, the density of states, and the absorption coefficient due to photoexcitation of localized electrons under THz or mid-IR excitation. We demonstrate that these properties are modified essentially under variation of the UNL's characteristics and we discuss possibilities for the verification of the transfer matrix parameters. In addition, formation of the localized state at a UNL and modification of propagation of electrons across UNLs (effective reflection from single UNL and miniband states of SL) lead to changes in both the transport properties and concentration of electrons. As a result, optoelectronic devices with UNLs should be analyzed by taking into account these factors.

The consideration below is organized as follows. In section 2 we describe a UNL in the framework of the transfer matrix approach. The single-layer case is considered in section 3 and the properties of SL formed by UNL are considered in section 4 (some details are in the appendix). A discussion of the experimental verification of the UNL's parameters is performed in section 5. Concluding remarks and a list of the assumptions used are given in section 6.

2. Transfer matrix approach

Within the one-band effective mass approximation, the electronic states in a bulk semiconductor with a UNL placed at $z = z_0$ is described by the Schrodinger equation:

$$\frac{\hat{p}_z^2}{2m}\Psi_z = E\Psi_z, \qquad z \neq z_0. \tag{1}$$

Here m is the effective mass and $\hat{p}_z$ is the momentum operator. The second-order differential equation (1) should be solved with the boundary conditions which connect the wavefunctions and their first derivatives at $z_0 - 0$ and $z_0 + 0$. Similarly to the consideration of an abrupt heterojunction case [7, 8], we write the connection rules for the column Φ_z in the form:

$$\Phi_{z_0+0} = \hat{T}\Phi_{z_0-0}, \qquad \Phi_z \equiv \begin{vmatrix} \Psi_z \\ \mathrm{d}\Psi_z/\mathrm{d}z \end{vmatrix}. \tag{2}$$

The 2×2 transfer matrix $\hat{T}$ is determined by the current conservation requirement and by the symmetry properties of layer.

From equation (1) it follows that $\widetilde{\Phi}_z^+\hat{\sigma}_y\Phi_z$ does not depend on z if $z \neq z_0$ (here and below $\hat{\boldsymbol{\sigma}}$ is the Pauli matrix which connects Ψ_z and its derivative). We impose the current conservation requirement at UNL as $\widetilde{\Phi}_z^+\hat{\sigma}_y\Phi_z|_{z_0-0}^{z_0+0} = 0$. Since two arbitrary states $\widetilde{\Phi}_z$ and Φ_z are considered here, the current conservation gives the condition for the transfer matrix:

$$\hat{T}^+\hat{\sigma}_y\hat{T} = \hat{\sigma}_y, \tag{3}$$

see similar evaluation for heterojunction in [8]. Further, we restrict ourselves to the case of symmetric UNL, when Φ_z and $\hat{\sigma}_z\Phi_{-z}$ should be determined by the same equations. As a result one obtains the additional condition:

$$\hat{\sigma}_z\hat{T}\hat{\sigma}_z = \hat{T}^{-1} \tag{4}$$

and the four complex parameters of $\hat{T}$ should be determined from the eight conditions given by equations (3) and (4). Straightforward calculations give us the transfer matrix[1]

$$\hat{T} = \begin{vmatrix} \tau & \tau_{12} \\ \tau_{21} & \tau \end{vmatrix}, \qquad \det\hat{T} = 1 \tag{5}$$

[1] Writing $\hat{T}$ through the Pauli matrix $\hat{T} = t + \mathbf{t}\cdot\hat{\boldsymbol{\sigma}}$ and using equation (4) one obtains $t_z = 0$ and $t^2 - (\mathbf{t}_\parallel \cdot \mathbf{t}_\parallel) = 1$. The current conservation (3) is valid if t and t_x are real but t_y is imaginary. As a result, $\hat{T}$ is determined through three real parameters, $\tau = t$, $\tau_{12} = t_x - \mathrm{i}t_y$, and $\tau_{21} = t_x + \mathrm{i}t_y$ with the additional condition $\det\hat{T} = 1$.

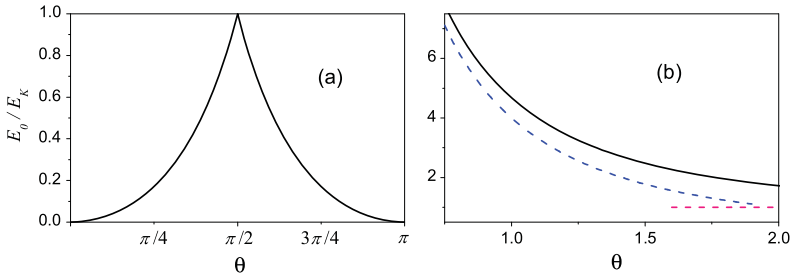

Figure 2. Dimensionless energy of localized state E_0/E_K versus phase Θ for the cases of $|\tau| < 1$ (a) and $\tau < -1$ (b). Dashed curves in panel (b) correspond to asymptotes at $\Theta \ll 1$ and $\Theta \gg 1$.

written through real parameters τ, τ_{12} and τ_{21}. Since the determinant is fixed here, the matrix $\hat{T}$ depends on two real parameters, which should be considered as phenomenological characteristics of UNL.

At $|\tau| < 1$, it is convenient to introduce the phase, Θ, and wavevector, K, so that the transfer matrix takes the form:

$$\hat{T} = \begin{vmatrix} \cos\Theta & K^{-1}\sin\Theta \\ -K\sin\Theta & \cos\Theta \end{vmatrix} \tag{6}$$

which depends on two phenomenological parameters, $K > 0$ and $0 < \Theta < 2\pi$. If $|\tau| > 1$, one can use similar expressions for $\hat{T}_\pm$, which is written through the hyperbolic functions:

$$\hat{T}_\pm = \begin{vmatrix} \pm\cosh\Theta & K^{-1}\sinh\Theta \\ K\sinh\Theta & \pm\cosh\Theta \end{vmatrix}. \tag{7}$$

Here the signs $+$ and $-$ correspond to $\tau > 1$ and $\tau < -1$, respectively. Once again, we suppose $K > 0$ in equation (7) because Θ can have any sign.

The explicit expressions for Θ and K can be written for $N \gg 1$, when $\hat{T}$ can be evaluated within the EMA approximation, for the wide layer cases (i) and (ii). For the N-monolayer well or barrier of the thickness Na with the band offset ΔU and the effective mass m_l, one obtains the transfer matrix $\hat{T}$ or $\hat{T}_+$ given by equations (6) and (7), respectively. The parameters Θ and K are determined by

$$\Theta = N\sqrt{\frac{m_l}{m}}Ka, \qquad E_K = \frac{(\hbar K)^2}{2m} = \frac{m}{m_l}\Delta U, \tag{8}$$

where the characteristic energy E_K is introduced. For the case of InAs well placed in GaAs [12] one obtains that the energy E_K varies between 1 and 2.8 eV, depending on the mismatch stress contributions. The phase Θ varies between $0.32N$ and $0.42N$, where $N \gg 1$ (for the case (i), Θ should be reduced to the interval $(0, 2\pi)$). Similar estimates can be obtained for other heterostructures with well-like or barrier-like UNL. Notice, that the non-conventional case $\tau < -1$ described by matrix $\hat{T}_-$ has no analogy with the results for well or barrier described by equations (8) within the EMA approximation.

3. Single-layer case

Here we consider the single UNL placed at $z_0 = 0$. The state localized along the $0Z$ direction, with energy $-E_0 < 0$, is described by the wavefunction

$$\Psi_z = \Psi_0[\theta(z)\mathrm{e}^{-\kappa z} + \theta(-z)\mathrm{e}^{\kappa z}], \qquad E_0 = \frac{(\hbar\kappa)^2}{2m}, \tag{9}$$

where $\theta(z)$ is the Heaviside step function, E_0 is the binding energy written through the characteristic size of localization, κ^{-1}, and $\Psi_0 = \sqrt{\kappa}$ is the normalization coefficient. The boundary condition (2) gives us the dispersion relation which determines $\kappa > 0$ through the transfer matrix parameters, Θ and E_K. As a result, at $\tau < 1$ the binding energy of localized state E_0 is given by:

$$E_0 = E_K \begin{cases} \left(\dfrac{\sqrt{1+\tan^2\Theta}-1}{\tan\Theta}\right)^2, & |\tau| < 1 \\ \left(\dfrac{\sqrt{1-\tanh^2\Theta}+1}{\tanh\Theta}\right)^2, & \tau < -1 \end{cases} \tag{10}$$

and there is no localized state for the barrier-like case $\tau > 1$.

In figure 2 we plot the dependences of E_0/E_K versus Θ. If $|\tau| < 1$ then $E_0/E_K < 1$, moreover a deep level with $E_0 \to E_K$ is realized at $\Theta \to \pi/2$ and such a dependency is plotted over the interval $(0, \pi)$ because it is a periodic function. At $\Theta \leq \pi/4$ or $\pi - \Theta \leq \pi/4$ a shallow state at UNL is realized. For a non-conventional UNL with $\tau \leq -1$, a deep level with $E_0/E_K > 1$ is realized and $E_0 \to E_K$ if $|\Theta| \gg 1$, while in the opposite case $|\Theta| \to 0$ one obtains the divergent asymptote $E_0/E_K \approx (2/\Theta)^2$. These asymptotes are also shown in figure 2(b).

The scattering problem, for an electron with energy $E > 0$ propagating from the left, is described by the wavefunction

$$\Psi_z = \theta(-z)(\Psi_\mathrm{i}\,\mathrm{e}^{\mathrm{i}kz} + \Psi_\mathrm{r}\,\mathrm{e}^{-\mathrm{i}kz}) + \theta(z)\Psi_\mathrm{t}\,\mathrm{e}^{\mathrm{i}kz}, \tag{11}$$

where $\Psi_\mathrm{i}, \Psi_\mathrm{r}$, and Ψ_t are the amplitudes of the incident, reflected, and transmitted waves. The wavevector k is connected with the energy E by the standard relation $E = (\hbar k)^2/2m$. The reflected and transmitted amplitudes, Ψ_r, and Ψ_t, are expressed through Ψ_i from the boundary condition (2). Further, we introduce the flows $J_\gamma = |\Psi_\gamma|^2\hbar k/m$, which correspond to the incident ($\gamma = \mathrm{i}$), reflected ($\gamma = \mathrm{r}$), and transmitted ($\gamma = \mathrm{t}$) waves, and calculate the reflection and transmission coefficients according to $R_E = J_\mathrm{r}/J_\mathrm{i}$ and $T_E = J_t/J_\mathrm{i}$. Since the particle conservation law, $R_E + T_E = 1$, only

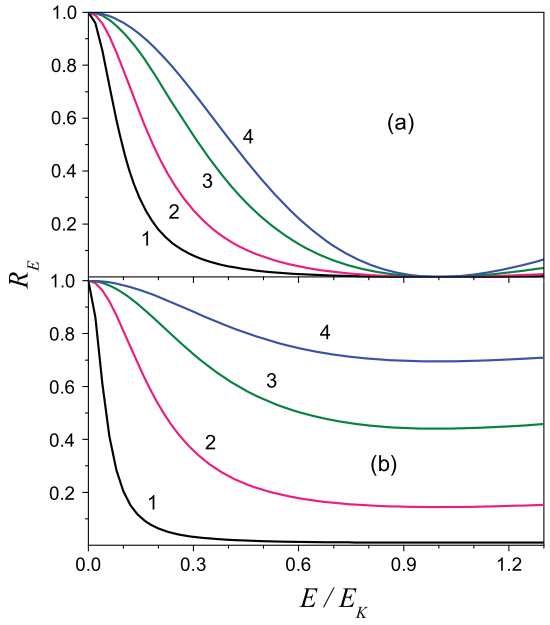

Figure 3. (a) Reflection coefficient R_E versus dimensionless energy E/E_K for the case $|\tau| < 1$ at $\Theta = \pi/16$ (1), $\pi/8$ (2), $\pi/4$ (3), and $\pi/2$ (4). (b) The same for the case $|\tau| > 1$ at $\Theta = 0.1$ (1), 0.4 (2), 0.8 (3), and 1.2 (4).

the reflection coefficient is considered below:

$$R_E = [1 + F(\Theta, k/K)]^{-1},$$
$$F(\Theta, z) = \begin{cases} \left[\dfrac{2z}{\sin\Theta(1-z^2)}\right]^2, & |\tau| < 1 \\ \left[\dfrac{2z}{\sinh\Theta(1+z^2)}\right]^2, & |\tau| > 1. \end{cases} \quad (12)$$

Here $F(\Theta, z) = F(-\Theta, z)$ and R_E is determined by positive Θ; the interval $0 < \Theta < \pi/4$ is enough in order to describe the case of UNL with $|\tau| < 1$.

Figure 3 shows the reflection coefficient R_E versus $E/E_K = (k/K)^2$. Since $F(\Theta, 0) = 0$, there is no tunneling of low-energy electrons through any UNL because $R_{E\to 0} \to 1$. If energy increases, R_E decreases up to $E = E_K$ and, once again, $R_E \to 1$ if $E \gg E_K$. But in the region $E \sim E_K$ the behavior of R_E is different for $|\tau| < 1$ and $|\tau| > 1$: the well-like case $R_{E_K} = 0$, while for $|\tau| < 1$ the reflection coefficient approaches constant, compare figures 3(a) and (b) (there is no difference between the cases (ii) and (iii) in panel (b)).

4. Superlattice

We turn now to the consideration of electronic states in SL of the period l formed by the UNLs placed at $z_0 \to \{nl\}$, $n = 0, \pm 1, \ldots$. Based on the boundary conditions (2) at $z = nl$, below we consider the miniband energy spectrum and calculate the absorption coefficient of doped SL under photoexcitation of localized states.

4.1. Miniband spectrum

The eigenvalue problem for the periodic system of UNLs is solved introducing a quasimomentum $0 < p_\perp < 2\pi\hbar/l$ and using Bloch's theorem, $\Psi_{p_\perp z} = \exp(\mathrm{i}p_\perp l/\hbar)\Psi_{p_\perp z-l}$. The wavefunction takes the form

$$\Psi_{p_\perp z} = \frac{N_{p_\perp}}{\sqrt{l}}[\mathrm{e}^{\mathrm{i}kz} + R(p_\perp, k)\mathrm{e}^{-\mathrm{i}kz}], \qquad 0 < z < l, \quad (13)$$

where $N_{p_\perp}$ is the normalization factor. By analogy with the general consideration [11], the coefficient $R(p_\perp, k)$ and the dispersion relation between $p_\perp$ and k are determined from the periodicity requirement and the boundary conditions (2) at $z = 0, l$, see appendix for details. For the UNL with $|\tau| < 1$ we use the transfer matrix (6) and the factor $R(p_\perp, k)$ takes the form

$$R(p_\perp, k) = \frac{\mathrm{e}^{\mathrm{i}p_\perp l/\hbar} - [\cos\Theta + (\mathrm{i}k/K)\sin\Theta\mathrm{e}^{\mathrm{i}kl}]}{\mathrm{e}^{\mathrm{i}p_\perp l/\hbar} - [\cos\Theta - (\mathrm{i}k/K)\sin\Theta\mathrm{e}^{-\mathrm{i}kl}]}, \quad (14)$$

while the dispersion equation is written as follows:

$$\cos\frac{p_\perp l}{\hbar} = \cos\Theta\cos kl - \frac{1}{2}\left(\frac{K}{k} + \frac{k}{K}\right)\sin\Theta\sin kl. \quad (15)$$

If $|\tau| > 1$ one uses the transfer matrix (7) and the factors $R_\pm(p_\perp, k)$ should be written similarly to equation (14) but through the hyperbolic functions, $\pm\cosh\Theta$ and $\sinh\Theta$ instead of $\cos\Theta$ and $\sin\Theta$. The corresponding dispersion equation is given by

$$\cos\frac{p_\perp l}{\hbar} = \pm\cosh\Theta\cos kl + \frac{1}{2}\left(\frac{K}{k} - \frac{k}{K}\right)\sinh\Theta\sin kl. \quad (16)$$

As in equation (7), here and in $R_\pm(p_\perp, k)$ the signs $+$ and $-$ correspond to $\tau > 1$ and $\tau < -1$, respectively. The last case has no analogy with the standard dispersion relations obtained in the EMA approximation, while equations (15) and (16) with $+\cosh\Theta$ are similar to the results for wells or barriers of finite width [11].

The contour plots of the right-hand sides of equations (15) and (16) versus Θ and dimensionless energy $E/\sqrt{E_K\varepsilon_l}$, (here $\varepsilon_l = (\hbar/l)^2/2m$ is a small energy corresponding to SL of period l) are presented in figure 4. Here the gap regions, which are above $+1$ and below -1, are shaded by gray and the dashed curves are plotted at the middle of miniband energies, when $\cos p_\perp l/\hbar = 0$. For the well-like case, $|\tau| < 1$, the weakly-coupled SL is realized if $\Theta \to 0, \pi, 2\pi$ and far from these points the tight-binding coupling regime takes place, see figures 4(a) and (b). With increasing of the dimensionless parameter $\sqrt[4]{E_K/\varepsilon_l}$, a number of minibands increases and a weakly-coupled regime is under more rigid conditions, compare figures 4(a) and (b). If $|\tau| > 1$ (i.e. SL is formed by barrier-like or non-conventional UNLs), the tight-binding regime of coupling takes place if $\Theta > 0.5$ and a weakly-coupled SL is realized at $\Theta \to 0$. Transformations between these regimes are different if $\tau > 1$ or $\tau < -1$, compare figures 4(c)and (d).

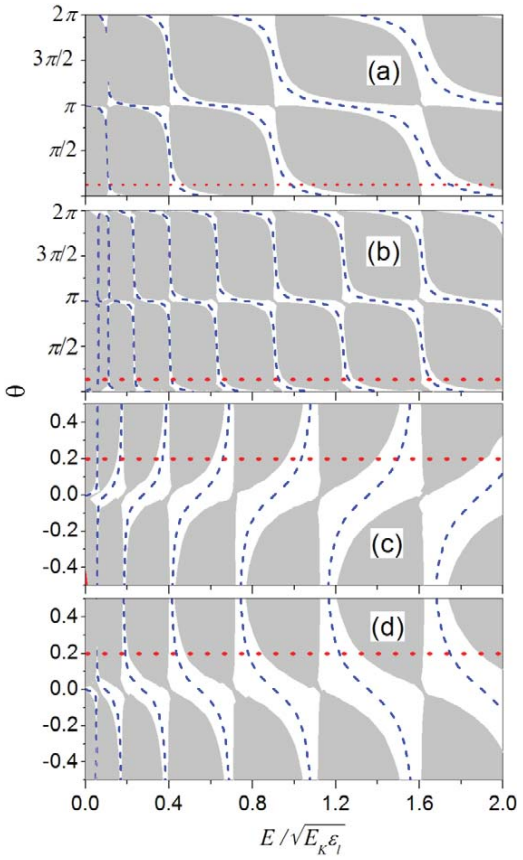

Figure 4. (a) Contour plot of the right-hand side of equation (15) versus Θ and dimensionless energy $E/\sqrt{E_K\varepsilon_l}$ at $\sqrt[4]{E_K/\varepsilon_l} = 10$. (b) The same as in panel (a) at $\sqrt[4]{E_K/\varepsilon_l} = 20$. (c) The same as in panel (a) for the dispersion equation (16) at $\tau > 1$ and $\sqrt[4]{E_K/\varepsilon_l} = 15$. (d) The same as in panel (c) at $\tau < -1$. Gap regions are shaded, dashed curves correspond to the zero level, and dotted lines correspond to the cross-sections shown in figure 5.

The dispersion laws $\varepsilon_{rp_\perp} = (\hbar k_{rp_\perp})^2/2m$, which are written through $k_{rp_\perp}$ determined by the dispersion equations (15) or (16) depending on UNL parameters, are shown in figure 5 at Θ marked in each panel of figure 4. The energy scale of gaps and allowed bands is determined by the characteristic energy $\sqrt{E_K\varepsilon_l}$, which is between 70 and 25 meV for $l = 10$–50 nm if E_K is taken as 1 eV. The dispersion laws plotted in figure 5 are close to cosine or sine dependences.

Further, we consider the density of states, which is introduced by the standard formula: $\rho_E = (2/L^3)\sum_\delta \delta(E-\varepsilon_\delta)$ where $\varepsilon_\delta \to \varepsilon_{rp_\perp} + \varepsilon_p$. Here we separated the in-plane kinetic energy, $\varepsilon_p = p^2/2m$, which corresponds to the 2D momentum **p**, and the superlattice contribution, $\varepsilon_{rp_\perp}$ plotted in figure 5. Integration over **p** gives the 2D density of states, ρ_{2D}, and ρ_E appears to be written through the integrals taken over the step function, $\theta(z)$:

$$\rho_E = \rho_{2D}\sum_r \int_0^{2\pi\hbar/l} \frac{dp_\perp}{2\pi\hbar}\theta(E-\varepsilon_{rp_\perp}). \qquad (17)$$

If E belongs to the $\bar r$th gap, the θ-functions for $r \le \bar r$ should be replaced by unity and ρ_E is constant. In the $\bar r$th miniband

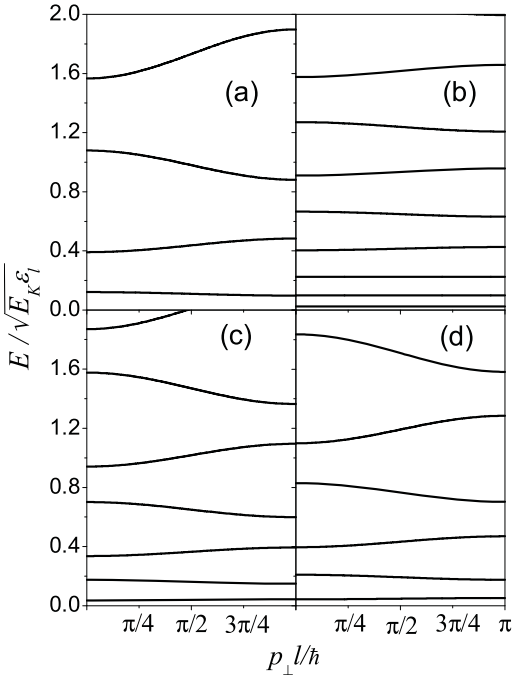

Figure 5. Miniband energy spectra $\varepsilon_{rp_\perp}$ for the parameters used in figures 4(a)–(d) at $\Theta = \pi/8$ (a), (b) and 0.2 (c), (d).

(below the rth gap), the integral over $p_\perp$ should be taken over the interval $(0, p_E)$, where p_E is found as a root of the equation $E = \varepsilon_{\bar r p_E}$. As a result, the density of states takes the form:

$$\rho_E = \frac{\rho_{2D}}{l}\begin{cases} \bar r, & E \subset \bar r\text{th gap} \\ \bar r - 1 + \dfrac{p_E l}{2\pi\hbar}, & E \subset \bar r\text{th miniband} \end{cases} \qquad (18)$$

and a ladder-like shape of ρ_E is determined by the gap-induced steps with miniband contributions between them.

In figure 6 we plot the density of states for the same parameters as in figure 5. Here the thick straight lines correspond to gap contributions, with miniband contributions between them which are similar to arccosine dependences. One can see that the number of minibands increases with the parameter $\sqrt[4]{E_K/\varepsilon_l}$. An approach to the square-root dependence, corresponding to the bulk density of states, takes place at $E/\sqrt{E_K\varepsilon_l} > 3$. Since ρ_E is connected directly to the shape of interband optical spectra, see [6b], the step-like dependences over the interval $E/\sqrt{E_K\varepsilon_l} \le 3$ permit one to extract UNL parameters which determine the bandstructure of SL. The effect of the above-barrier states on PLE spectra in the wide InGaAs/GaAs structure was measured and calculated within the EMA approach in [12].

4.2. Absorption coefficient

Using the solutions obtained, we consider below the process of photoexcitation of electrons localized at levels of energy $-E_0$ into minibands caused by the radiation polarized along SL axis. Such absorption takes place in heavily doped SL formed by the well-like or non-conventional UNLs; we do not

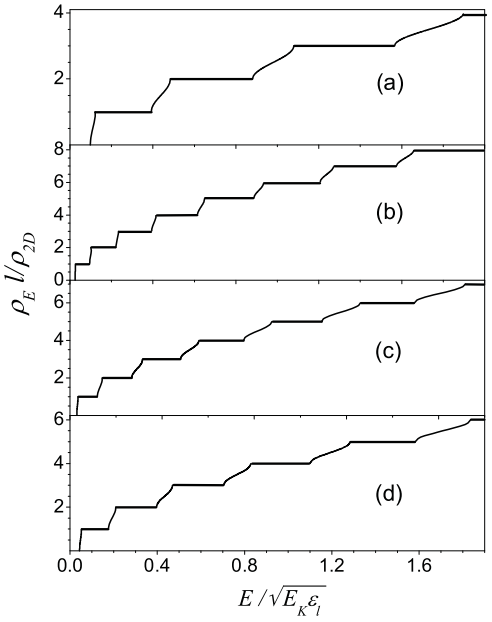

Figure 6. Normalized density of states for the parameters used in panels (a)–(d) of figures 4 and 5.

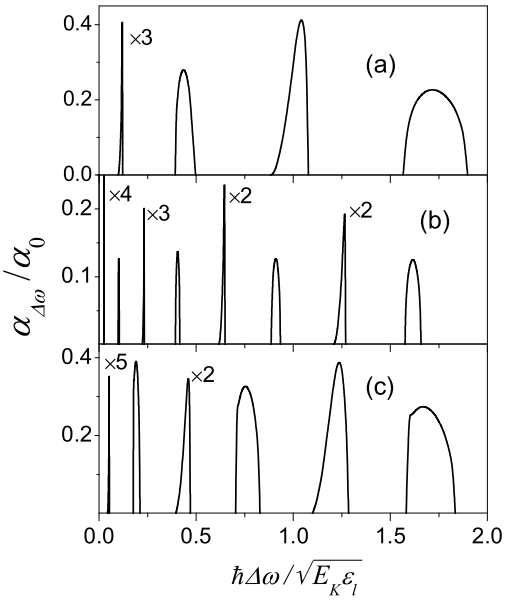

Figure 7. (a) Spectral dependences of dimensionless absorption coefficient $\alpha_{\Delta\omega}/\alpha_0$ for $\Theta = \pi/12$ at the same conditions as in figures 4(a)–6(a). (b) The same as in panel (a) for the conditions of figures 4(b)–6(b). (c) The same as in panels (a), (b) for $\Theta = 0.1$ and the conditions of figures 4(d)–6(d).

consider here the case (ii), which is similar to an ordinary SL, see [13]. The absorption coefficient α_ω is determined by the general Kubo formula as follows:

$$\alpha_\omega = \frac{8(\pi e)^2}{\sqrt{\epsilon}c\omega L^3}\sum_{\delta\delta'}[f(\varepsilon_\delta) - f(\varepsilon_\delta + \hbar\omega)]\left|(\delta|\hat{v}_z|\delta')\right|^2 \times \delta\left(\varepsilon_\delta - \varepsilon_{\delta'} + \hbar\omega\right), \tag{19}$$

where ϵ is the dielectric permittivity of the host semiconductor, L^3 stands for the normalization volume, and the matrix element $\left|(\delta|\hat{v}_z|\delta')\right|^2$ corresponds to transitions between δ- and δ'-states of energies ε_δ and $\varepsilon_{\delta'}$. We use the equilibrium distribution $f(\varepsilon_\delta)$ and take into account $\varepsilon_\delta \to \varepsilon_p - E_0$ because only localized states are populated. Since transitions are vertical, the energy conservation law and the matrix element do not depend on $\mathbf{p}$ and the 2D concentration $n_{2D} = (2/L^2)\sum_{\mathbf{p}} f(\varepsilon_p - E_0)$ appears in (19) if $\hbar\omega > E_0$. In addition, the matrix element $M_{rp_\perp} = \left|(0|\hat{v}_z|rp_\perp)\right|^2$ is the same for any UNL and (19) may be transformed into the sum over different minibands

$$\alpha_\omega = \frac{2\pi e^2 n_{2D}}{\sqrt{\epsilon}c\hbar\omega}\sum_{\mathrm{r}}\int_0^{2\pi\hbar/l} \mathrm{d}p_\perp\, M_{rp_\perp}\delta(\hbar\Delta\omega - \varepsilon_{rp_\perp}) \tag{20}$$

written through the frequency detuning, $\Delta\omega = \omega - E_0/\hbar$.

The transparency regions take place if $\hbar\Delta\omega$ belongs to any gap. If $\hbar\Delta\omega$ is brought into the $\bar{r}$th miniband, the corresponding absorption coefficient takes the form

$$\alpha_\omega^{(\bar{r})} = \frac{2\pi e^2 n_{2D}}{\sqrt{\epsilon}c\hbar\omega}\frac{M_{\bar{r}p_{\Delta\omega}}}{|\mathrm{d}\varepsilon_{\bar{r}p_\perp}/\mathrm{d}p_\perp|_{p_{\Delta\omega}}}, \tag{21}$$

where $p_{\Delta\omega}$ should be determined from the equation $\hbar\Delta\omega = \varepsilon_{rp_{\Delta\omega}}$. Under the condition $\kappa l \gg 1$, the matrix element $M_{rp_\perp}$ is written through the wavefunctions (9) and (14) in the form (see appendix):

$$M_{rp_\perp} = \left(\frac{\hbar}{m}\right)^2\frac{\kappa}{l}\left|N_{p_\perp}\right|^2|1 + \mathrm{e}^{\mathrm{i}kl} + R\,(p_\perp, k)\,(1 + \mathrm{e}^{-ikl})|^2 \tag{22}$$

for the UNL with $|\tau| < 1$. If $|\tau| > 1$ one should use $R_\pm\,(p_\perp, k)$ in equation (22). Notice that $M_{rp_\perp}$ and the velocity $\mathrm{d}\varepsilon_{\bar{r}p_\perp}/\mathrm{d}p_\perp$ vanish at the edges of minibands, so that jumps of absorption are possible at edges of absorption regions. Thus, spectral dependences of $\alpha_\omega^{(\bar{r})}$ appear to be strongly dependent on the transfer matrix parameters and they can be extracted from these data.

The shapes of absorption peaks are determined by equations (21) and (22) and by the dispersion relations $\varepsilon_{\bar{r}p_\perp}$, as is shown in figure 7 for lower peaks. Here we plotted the dimensionless spectral dependences $\alpha_{\Delta\omega}/\alpha_0$, where

$$\alpha_0 = \frac{8\pi e^2}{\sqrt{\epsilon}c}n_{2D}\sqrt{\frac{2}{mE_0}} \tag{23}$$

is the characteristic absorption. For the case of IR absorption of SL with concentration $n_{2D} = 5 \times 10^{11}$ cm^{-2} and $E_0 \sim 0.1$ eV,[2] one obtains $\alpha_0 \simeq 1.25 \times 10^4$ cm^{-1} if $\sqrt{\epsilon} \simeq 3.3$. The positions and widths of absorption peaks correspond to the miniband energy spectra shown in figures 4 and 5. There is an essential difference between odd and even peaks due to the inversion symmetry of the eigenstate problem at the edges of minibands, when $p_\perp l/\hbar = 0, 2\pi$. The odd peaks

[2] This value is taken in agreement with experimental data of [14].

are non-symmetric ones, they are higher (see the scaling factors in figure 7) and more narrow in comparison to the even peaks, which are more symmetric and wide. Since the condition $\kappa l > 1$ is satisfied at $l \geq 10$ nm, a visible (>30%) absorption takes place for a 20-layer periodic structure and the mid-IR measurements permit a direct verification of the SL parameters.

5. Experimental verification

Next, we briefly discuss the possibilities for experimental verification or for *ab initio* calculations of the UNL's parameters. It is not a simple task because the UNL's parameters affect the response of the heterostructure in a complicated way and one needs to design an appropriate structure and to perform special measurements. Also, any first-principles calculations of the UNL's parameters should include both UNL and host material, so that it is necessary to perform calculations on an atomic level for a long-period SL in order to compare with the results of section 4 written through the UNL's parameters. Any method used for short-period SL, see [9] and references therein, can be applied providing a generalization for the case of a long host material. Similar calculations for InAs UNL embedded by GaAs together with the measurements of capacitance–voltage characteristics were performed in [14] and the binding energy of localized state E_0 appears to be ∼60 meV. This value is about three times smaller than the EMA estimate of E_0 given by equations (8) and figure 2(a). Thus, the EMA approach is not valid for the description of the InAs UNL in GaAs host matrix but a complete determination of parameters Θ and E_K is not possible due to lack of data in [14].

Below we list a set of papers, where UNLs based on different heteropairs were realized, and discuss possible measurement schemes in order to verify the UNL parameters. Different optoelectronic devices contain quantum dot sheets with an ultranarrow wetting layer [1–4] and the influence of these layers on electronic states is described by the results obtained here if one neglects the quantum dots effect. UNLs with $N \sim 5$ are widely used in the quantum cascade lasers [15], where each period contains about ten layers of different thickness, so that a verification of the UNL parameters is difficult. At least several measurements of InAs UNLs placed into GaAs or AlGaAs matrix [16] as well as results for UNLs in $A_{\rm IV}B_{\rm VI}$ [17] and in $A_{\rm II}B_{\rm VI}$ [18] heterostructures have been published. But a verification of UNL parameters was not performed in these papers and a special investigation for each system is necessary.

All the results obtained in section 4 depend strongly on Θ and E_K, which determine the transfer matrices (6) or (7), and these parameters can be verified from the spectroscopical measurements. Indeed, the results of section 4.2 demonstrate that mid-IR (or THz, depending on parameters in question) absorption is strongly varied depending on transfer matrix parameters. The near-IR interband transitions in SL depend essentially on the density of states considered in section 4.1 for different UNL parameters. Variations of the near-IR spectra from the bulk case permit one to verify Θ and E_K using the electromodulation spectroscopy or the PLE measurements. Besides this, the transfer matrix parameters can be extracted from the transport data, but in addition to the UNL parameters, some other characteristics, e.g. scattering rates, should be involved in interpretation of these data.

6. Conclusions

In summary, we have re-examined the theory of electronic states in heterostructures formed by ultranarrow layers, taking into account that the EMA approximation cannot be applied for description of UNLs. Our consideration is based on the transfer matrix method, which was generalized for the case of UNL. It is found that three types of UNL are possible, depending on the value of the diagonal element in the transfer matrix (5). The cases $|\tau| < 1$ or $\tau > 1$ are similar to a narrow well or barrier, while there is no simple analogy with a wide layer for the non-conventional UNL with $\tau < -1$. The localized level appears at a single UNL with $\tau < 1$. The energy-dependent reflection coefficients of a single UNL as well as the energy spectrum of SL formed by a periodic array of UNLs are different for the cases $|\tau| < 1$ and $\tau > 1$. The spectral dependences of absorption are analyzed for the case of photoexcitation of localized electrons into the SL's minibands. The EMA approach fails to explain the results of [14], but there is a lack of experimental data for verification of the UNL parameters.

Let us discuss now the main assumptions applied to the consideration performed. Using the single-band Hamiltonian in equation (1) we suppose that the electron energy E is small in comparison with the gap of the host semiconductor. In order to consider the high-energy states, one needs to use the **kp**-Hamiltonian and more complicated boundary conditions, see similar considerations of an abrupt heterojunction in [8, 20]. In addition, the transfer matrix approach is valid for the description of UNL of width Na if Na is less than the electron wavelength, i.e. $(\hbar/Na)^2/2m \gg E$. We restrict ourselves to the model of symmetric UNL based on the condition (4). It should be mentioned that the EMA-based estimates given by equations (8) are not valid for $N \sim 1$, at least for InAs UNLs, see the discussion in [19], and equations (8) can be used if $Na > 10$ Å. A more complicated consideration is necessary in order to take into account a non-symmetry of UNL; this case should be considered elsewhere. Also, we consider an ideal UNL, neglecting an in-plane scattering processes or inhomogeneous broadening; this approximation is valid if E exceeds a typical broadening energy. A possible segregation of UNLs (some experimental data for InAs see in [21]) will not be essential because short-scale lateral inhomogeneities are realized. In the structures with quantum dots formed over wetting layers, an additional contribution from dot-induced scattering should be essential [22].

To conclude, we believe that the results obtained will stimulate the verification of phenomenological parameters describing the electronic properties of UNLs using mid-IR spectroscopy when the valence band states are not essential. These data should be important for applications of heterostructures with UNLs in different devices.

Acknowledgment

This work was supported by the AFOSR.

Appendix

We consider here the eigenstate problem for the SL formed by UNLs in more detail. SL states are described by the Schrodinger equation $(\hat{p}_z^2/2m)\Psi_z = E\Psi_z$ which should be solved with the boundary condition at $z_n = nl$ with $n = 0, \pm 1, \ldots$

$$\left|\begin{matrix}\psi_z \\ \mathrm{d}\psi_z/\mathrm{d}z\end{matrix}\right|_{z_n+0} = \hat{T}\left|\begin{matrix}\psi_z \\ \mathrm{d}\psi_z/\mathrm{d}z\end{matrix}\right|_{z_n-0}, \qquad (A.1)$$

which is written through the transfer matrix $\hat{T}$ given by equations (5)–(7). According to Bloch's theorem $\exp(-\mathrm{i}p_\perp z/\hbar)\psi_z$ is a periodic function, so that the wavefunction corresponding to the quasimomentum $p_\perp$ takes the form

$$\psi_{p_\perp z} = \begin{cases} \psi_{p_\perp}^{(+)}\mathrm{e}^{\mathrm{i}kz} + \psi_{p_\perp}^{(-)}\mathrm{e}^{-\mathrm{i}kz}, & |z| < \dfrac{l}{2} \\ \mathrm{e}^{\mathrm{i}p_\perp l/\hbar}[\psi_{p_\perp}^{(+)}\mathrm{e}^{\mathrm{i}k(z-l)} + \psi_{p_\perp}^{(+)}\mathrm{e}^{-\mathrm{i}k(z-l)}], & \dfrac{l}{2} < z < \dfrac{3l}{2}, \end{cases} \qquad (A.2)$$

where $\hbar k = \sqrt{2mE}$. The amplitudes $\psi_{p_\perp}^{(\pm)}$ in (A.2) are determined from the boundary condition

$$\left|\begin{matrix}\psi_z \\ \mathrm{d}\psi_z/\mathrm{d}z\end{matrix}\right|_{l/2+0} = \hat{T}\left|\begin{matrix}\psi_z \\ \mathrm{d}\psi_z/\mathrm{d}z\end{matrix}\right|_{l/2-0}, \qquad (A.3)$$

which is transformed into the linear system of equations for $\psi_{p_\perp}^{(\pm)}$. The solvability condition gives us the dispersion relations (15) and (16) for the cases $|\tau| < 1$ and $|\tau| > 1$, respectively. The eigenfunction (A.3) takes the form (13) with the normalization factor $N_{p_\perp}$ determined from $\int_{|z|<l/2}\mathrm{d}z\,|\psi_{p_\perp z}|^2 = 1$.

The matrix element of equation (20), which determines photoexcitation from the ground state into the rth miniband, is expressed through the wavefunctions (9) and (A.2) as follows

$$M_{rp_\perp} = \Psi_0^2\left(\frac{\hbar}{m}\right)^2\left|\psi_{rp_\perp z=l/2} + \psi_{rp_\perp z=-l/2}\right|^2. \qquad (A.4)$$

Here we have neglected overlap between states localized at different UNLs. After substitution of the wavefunction (13) and straightforward algebra one arrives at the result given by equation (22).

References

[1] Zory P S (ed) 1993 *Quantum Well Lasers* (New York: Academic)
[2] Gmachl C, Capasso F, Sivco D L and Cho A Y 2001 *Rep. Prog. Phys.* **64** 1533
[3] Rogalski A 2003 *J. Appl. Phys.* **93** 4355
Pan J N and Fonstad C G 2000 *Mater. Sci. Eng.* **28** 65
[4] Avrutin V, Izyumskaya N and Morkoc H 2011 *Superlatt. Microstruct.* **49** 337
Brown G F and Wu J Q 2009 *Laser Photon. Rev.* **3** 394
[5] Bimberg D, Grundmann M and Ledentsov N N 1999 *Quantum Dot Heterostructures* (New York: Wiley)
Krestnikov I L, Ledentsov N N, Hoffmann A and Bimberg D 2001 *Phys. Status Solidi* a **183** 207
[6a] Bastard G 1988 *Wave Mechanics Applied to Semiconductor Heterostructures* (Paris: Editions de Physique)
[6b] Vasko F T and Kuznetsov A 1998 *Electronic States and Optical Transitions in Semiconductor Heterostructures* (New York: Springer)
[7] Ando T and Mori S 1982 *Surf. Sci.* **113** 124
Sokolov I M 1985 *Zh. Eksp. Teor. Fiz.* **89** 556
Sokolov I M 1985 *Sov. Phys. JETP* **62** 317 (Engl. transl.)
Laikhtman B 1992 *Phys. Rev.* B **46** 4769
[8] Tokatly I V, Tsibizov A G and Gorbatsevich A A 2002 *Phys. Rev.* B **65** 165328
[9] Donetsky D, Svensson S P, Vorobjev L E and Belenky G 2009 *Appl. Phys. Lett.* **95** 212104
Li H, Katz S, Boehm G and Amann M-C 2011 *Appl. Phys. Lett.* **98** 131113
[10] Schmidt H, Pickenhain R and Bohm G 2002 *Phys. Rev.* B **65** 045323
[11] Herman M 1986 *Semiconductor Superlattices* (Berlin: Academic)
Mitin V, Sementsov D and Vagidov N 2010 *Quantum Mechanics for Nanostructures* (Cambridge: Cambridge University Press)
[12] Worren T, Ozanyan K B, Hunderi O and Martelli F 1998 *Phys. Rev.* B **58** 3977
[13] Shik A Ya 1974 *Sov. Phys.—Semicond.* **8** 1841
Shik A Ya 1972 *Sov. Phys.—Semicond.* **6** 1110
Kastalsky A, Duffield T, Allen S J and Harbison J 1988 *Appl. Phys. Lett.* **52** 1320
[14] Pickenhain R, Schmidt H and Gottschalch V 2000 *J. Appl. Phys.* **88** 948
[15] Cathabard O, Teissier R, Devenson J, Moreno J C and Baranov A N 2010 *Appl. Phys. Lett.* **96** 141110
Revin D G, Commin J P, Zhang S Y, Krysa A B, Kennedy K and Cockburn J W 2011 *IEEE J. Quantum Electron.* **17** 1417
[16] Guimard D, Morihara R, Bordel D, Tanabe K, Wakayama Y, Nishioka M and Arakawa Y 2010 *Appl. Phys. Lett.* **96** 203507
Di Ventra M and Mader K A 1997 *Phys. Rev.* B **55** 13148
[17] Jeffers J D, Namjou K, Cai Z, McCann P J and Olona L 2011 *Appl. Phys. Lett.* **99** 041903
[18] Ivanov S V, Toropov A A, Shubina T V, Sorokin S V, Lebedev A V, Sedova I V, Kopev P S, Pozina G R, Bergman J P and Monemar B 1998 *J. Appl. Phys.* **83** 3168
[19] Paki P, Leonellia R, Isnard L and Masut R A 1999 *Appl. Phys. Lett.* **74** 1445
Albe V and Lewis L J 2001 *Physica* B **301** 233
[20] Kisin M V, Gelmont B L and Luryi S 1998 *Phys. Rev.* B **58** 4605
[21] Martini S, Manzoli J E and Quivy A A 2010 *J. Vac. Sci. Technol.* B **28** 277
Ares R, Tran C A and Watkins S P 1995 *Appl. Phys. Lett.* **67** 1576
[22] Vasko F T and Mitin V V 2012 *Phys. Rev.* B **85** 235321